High-volumetric-capacity WSe_2 Anode for Potassium-ion Batteries①

CHEN Ming[a, b] ZHAO Jun-Mei[c] SUN Chuan-Fu[b, d②]

[a] (*College of Chemistry and Materials Science, Fujian Normal University, Fuzhou* 350007, *China*)

[b] (*CAS Key Laboratory of Design and Assembly of Functional Nanostructures,and Fujian Key Laboratory of Nanomaterials, Fujian Institute of Research on the Structure of Matter, Chinese Academy of Sciences, Fuzhou* 350002, *China*)

[c] (*Innovation Academy for Green Manufacture, Chinese Academy of Sciences, Beijing* 100190, *China*)

[d] (*University of Chinese Academy of Sciences, Beijing* 100039, *China*)

ABSTRACT Exploring high-capacity electrode materials is critical for the development of K-ion batteries. In this work, we report a layered-structured tungsten selenide (WSe_2) anode, which not only delivers an ultrahigh volumetric capacity of 1772.8 Ah/L (or 188.4 mAh/g) at a current density of 5 mA/g but also exhibits good rate capability (72 mAh/g at 200 mA/g) and cycling stability (83.14% capacity retention over 100 cycles at 100 mA/g). We have also revealed the underlying reaction mechanism through ex situ X-ray powder diffraction. Furthermore, proof-of-concept full-cell batteries comprising of WSe_2 anodes and Prussian Blue cathodes are capable of delivering an energy density of 135.2 $Wh/kg_{cathode+anode}$. This work highlights the potential of WSe_2 as a promising high-volumetric-capacity anode material for rechargeable potassium-ion batteries.

Keywords: tungsten selenide, potassium-ion batteries, high volumetric capacity, conversion reaction;

DOI: 10.14102/j.cnki.0254–5861.2011–3106

1 INTRODUCTION

Lithium-ion batteries (LIBs) have been widely used in portable electronics and electric vehicles because of their high energy and power density[1, 2]. However, large-scale applications of LIBs for energy storage are seriously limited by the scarce reserves and uneven distribution of lithium resources[3]. Given the earth-abundant potassium resources and a similarly low redox potential of K/K^+ as Li/Li^+ (–2.93 V and –3.04 V, *vs* standard hydrogen electrode), potassium-ion batteries (KIBs)[4, 5] have been recognized as promising alternatives or supplements to LIBs for large-scale energy storage system[6, 7]. Despite tremendous potential, the development of KIBs has been largely hindered by the lack of suitable high-capacity electrode host materials. The (de)intercalation of the large-size K^+ ions often results in obvious structural degradation and therefore short cycle life to the electrode materials. On the other hand, the large ionic size typically leads to sluggish K^+-diffusion kinetics within the electrode materials and undesired fast-charging capability. Therefore, it is critical to search for new host materials that can not only store a large amount of K^+ ions reversibly but also exhibit fast reaction kinetics.

Layered-structured transition metal dichalcogenides (TMDs), such as MoS_2[8] and WS_2[9], have received considerable attention as promising KIBs anode materials as they operate based on conversion-type reactions and are capable of delivering high theoretical capacities[10, 11]. Very recently, Jiao *et al.* reported the anode behavior of a WSe_2/N-doped porous carbon composite (WSe_2/N-PC)[12]. Differing from the MoS_2 and WS_2 anodes that exhibit flat voltage plateaus and relatively long cycle life, the WSe_2 nanocomposite exhibits a high capacitive-dominated K^+-ion storage capacity without obvious voltage plateaus and limited cycle life. It is reasonably speculated the nanostructuring of WSe_2 is responsible for these discrepancies. Considering this，

Received 20 January 2021; accepted 21 February 2021

① This project was supported by the National Natural Science Foundation of China (Nos. 21771180, 21971239) and Natural Science Foundation of Fujian Province (No. 2020J06032)

② Corresponding author. E-mail: cfsun@fjirsm.ac.cn

it is necessary to investigate the intrinsic K^+-ion storage behavior of WSe_2 anode material and further improve its cycling stability.

Here we report a systematic investigation on the K^+-ion storage behavior of the pure WSe_2. We reveal that WSe_2, serving as an anode material for KIB, operates at an average potential of 0.85 V (versus K/K^+) accompanied by a flat voltage plateau and delivers an ultrahigh volumetric capacity of 1772.8 Ah/L at a current density of 5 mA/g. Moreover, the WSe_2 anode exhibits good rate capability (72 mAh/g at 200 mA/g) and long-term cycling stability (112 mAh/g remained over 100 cycles at 100 mA/g). Ex-situ X-ray powder diffraction analysis reveals that WSe_2 anode first undergoes intercalation reactions and then follows reversible conversion reactions. We have further fabricated full-cell KIBs utilizing a WSe_2 anode and a Prussian Blue cathode. The proof-of-concept batteries deliver a high energy density of 135.2 $Wh/kg_{cathode+anode}$. WSe_2 may open new opportunities for the development of high-capacity electrode materials adopted for high-energy-density rechargeable potassium-ion batteries.

2 EXPERIMENTAL

2. 1 Materials

WSe_2 powders (99.8% metals basis, CAS registry number: 12067-46-8) were purchased from Shanghai Macklin Biochemical Co., Ltd. Sodium carboxymethylcellulose (CMC) and Super-P carbon black were purchased from Hefei Kejing Materials Technology Co., Ltd. Battery grade potassium bis(trifluoromethylsulfonyl) imide (KTFSI) and diethylene glycol dimethyl ether (DEGDME, water content < 1 ppm) were purchased from DoDoChem. KTFSI was vacuum dried at 100 ℃ for 48 h before dissolving in DEGDME solvent.

2. 2 Materials characterization

X-ray powder diffraction (XRD) patterns were collected on a Rigaku Ultima IV X-ray diffractometer with Cu$K\alpha$ radiation source (λ = 1.54184 Å) at a 2θ range of 5～80° and a scanning rate of 1 °/min. The operating voltage and current are 40 kV and 40 mA, respectively. The microscopic size and morphology of WSe_2 were characterized by a field-emission scanning electron microscope (FESEM, HITACHI SU-8010).

2. 3 Electrochemical measurements

The WSe_2 electrode was prepared through a slurry blade-coating method. Specifically, the WSe_2 powders, carboxymethylcellulose (CMC) binder, and Super-P carbon black were mixed homogeneously with a mass ratio of 8:1:1 in deionized water. The slurry was coated on an Al foil and dried under vacuum at 80 ℃ for 12 h. The mass loading of WSe_2 is ～ 2.5 mg/cm^2. To investigate the electrochemical performance of WSe_2 electrode, the standard CR2032-type coin half cells were assembled with potassium metal foils as counter electrodes in an argon-filled glove-box. 5 M potassium bis(trifluoromethylsulfonyl)imide (KTFSI) in diethylene glycol dimethyl ether (DEGDME) was adopted as electrolytes[13] and glass fibers (Grade GF/F, Whatman) were applied as separators. Galvanostatic charge/discharge cycling tests at different current densities were carried out on LANHE CT-2001A in the voltage range of 0.1 to 2 V (*vs.* K/K^+). Cyclic voltammetry (CV) was performed on an electrochemical workstation (Bio-Logic SP-300) at a scanning rate of 0.1 mV/s in the voltage range of 0.1 to 3 V (*vs.* K/K^+). All electrochemical tests were conducted at a constant temperature of 28 ℃.

3 RESULTS AND DISCUSSION

As illustrated in Fig. 1a, WSe_2 exhibits a distinct layered structure with neighboring layers interconnected *via* Van der Waals force. The interlayer spacing of 6.49 Å is larger than those of ReS_2[14], MoS_2[8], WS_2[9], $NbSe_2$[15] and $ReSe_2$[16] (Fig. 1b), and favors the intercalation of large-ionic-size K^+ ions[17]. The crystal structure and phase purity are confirmed by X-ray powder diffraction (XRD). As shown in Fig. 1c, all the diffraction peaks could be accurately indexed to the standard WSe_2 structure (ICSD-40752) with space group *P*63/*mmc* (No. 194). The distinct Bragg peaks at 13.62°, 31.40°, 32.17°, 37.80°, and 41.70° correspond to (002), (100), (101), (103), and (006) lattice planes, respectively, with a highly preferred orientation in the (002) lattice plane. Scanning electron microscopy (SEM) imaging reveals that WSe_2 exhibits hexagon plate-like morphology with a lateral size of about ～100～200 nm and a thickness of ～30 nm (Fig. 1d).

The electrochemical behaviors of WSe_2 were explored by cyclic voltammetry (CV) and galvanostatic charge-discharge cycling tests. Fig. 2a shows the three-cycle CV curves collected at a scan rate of 0.1 mV/s within 0.01～3 V (*vs.* K/K^+). The irreversible reduction peak at ～0.45 V in the first cycle can be attributed to the formation of a solid electrolyte interphase (SEI)[18, 19]. In the following cycles, three pairs of reduction/oxidation peaks appearing at

1.16/1.18, 1.6/2.0 and 1.91/2.68 V indicate reversible K^+-ion insertion and extraction within WSe_2. Fig. 2b depicts the galvanostatic voltage profiles of WSe_2 at a current of 5 mA/g. WSe_2 delivers an initial discharging capacity of 297 mAh/g and a reversible charging capacity of 188.4 mAh/g as well as an initial Coulombic Efficiency (CE) of 61.9%. The irreversible capacity loss during the first cycle coincides with those observed in CV analysis and could be attributed to the formation of SEI, which is commonly observed in KIB anodes[20-23]. The volumetric capacity is estimated to be as high as 1772.8 Ah/L according to a density of 9.39 g/cm^3 for WSe_2, exceeding previously reported anode materials including graphitic carbon, organics, Ti-based compounds, metal sulfides as well as alloy-type P and Sn[8, 9, 13, 15, 24-34] (Fig. 2c). Figs. 2b and 2d depict the long-term cycling performance of the WSe_2 anode at 5 mA/g. WSe_2 still delivers a specific capacity of 144.4 mAh/g after 50 cycles, corresponding to a capacity retention of 76.4%. Equally importantly, the flat voltage plateau remains during 50 cycles (Fig. 2d), demonstrating the high reversibility of this new K^+-WSe_2 electrochemistry. At a current density of 20 mA/g, the WSe_2 anode delivers a reversible capacity of 117.4 mAh/g after 100 cycles and an average CE of 98.68% (Fig. 2e). At even higher current densities of 50 and 100 mA/g, capacities of 101.7 and 112 mAh/g are achieved after 100 cycles (Fig. 2f), respectively, with capacity retention (70.6% and 83.14%) exceeding that for previously reported WSe_2/N-PC (64% over 100 cycles at 100 mA/g)[12]. Moreover, the WSe_2 anode delivers a higher initial CE of 61.9% (versus 50.06% for WSe_2/N-PC).

Apart from good long-term cyclability, the WSe_2 anode also exhibits good rate capability. As shown in Figs. 2g and 2h, the WSe_2 anode delivers capacities of 183, 170, 151, 138, 107, 82, and 72 mAh/g at current densities of 5, 10, 20, 30, 50, 100, and 200 mA/g, respectively, and the voltage plateaus remain during rate-capability cycling. Equally importantly, the capacity recovers to 166 mAh/g when switching the current density back to 5 mA/g, manifesting the high reversibility of the WSe_2 anode against both deep and fast charging.

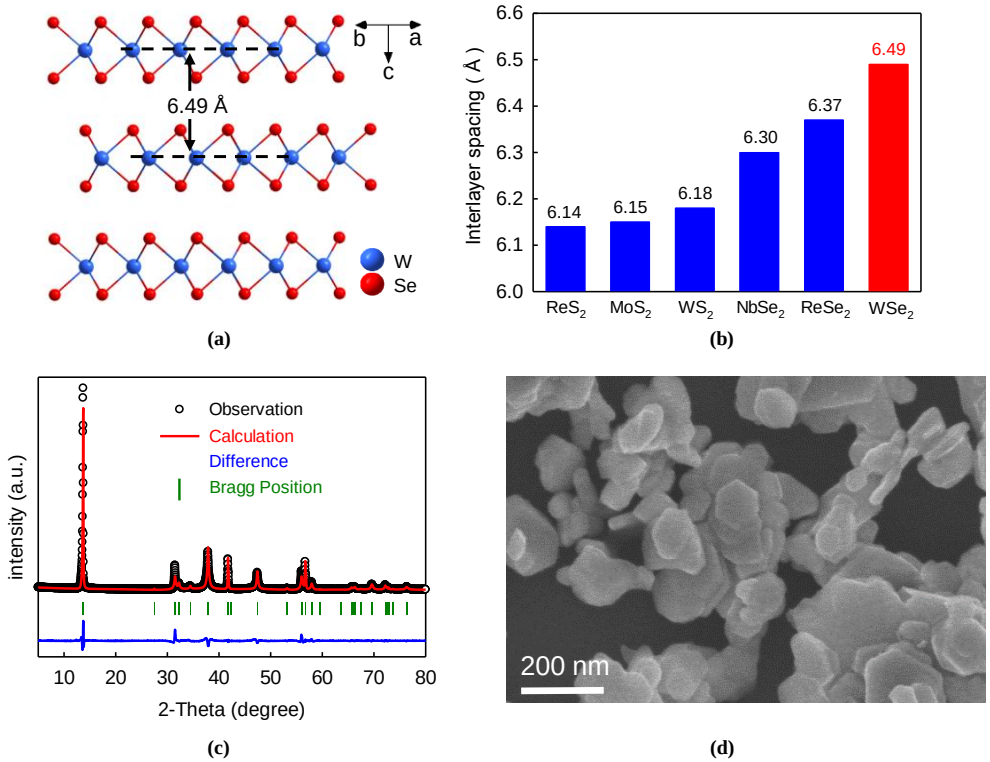

Fig. 1. (a) Crystal structure of WSe_2; (b) Comparison of interlayer spacing among TMDs; (c) Rietveld refinement of the XRD pattern of WSe_2 (R_{wp} = 9.69%, and R_p = 7.26%); (d) SEM image of WSe_2

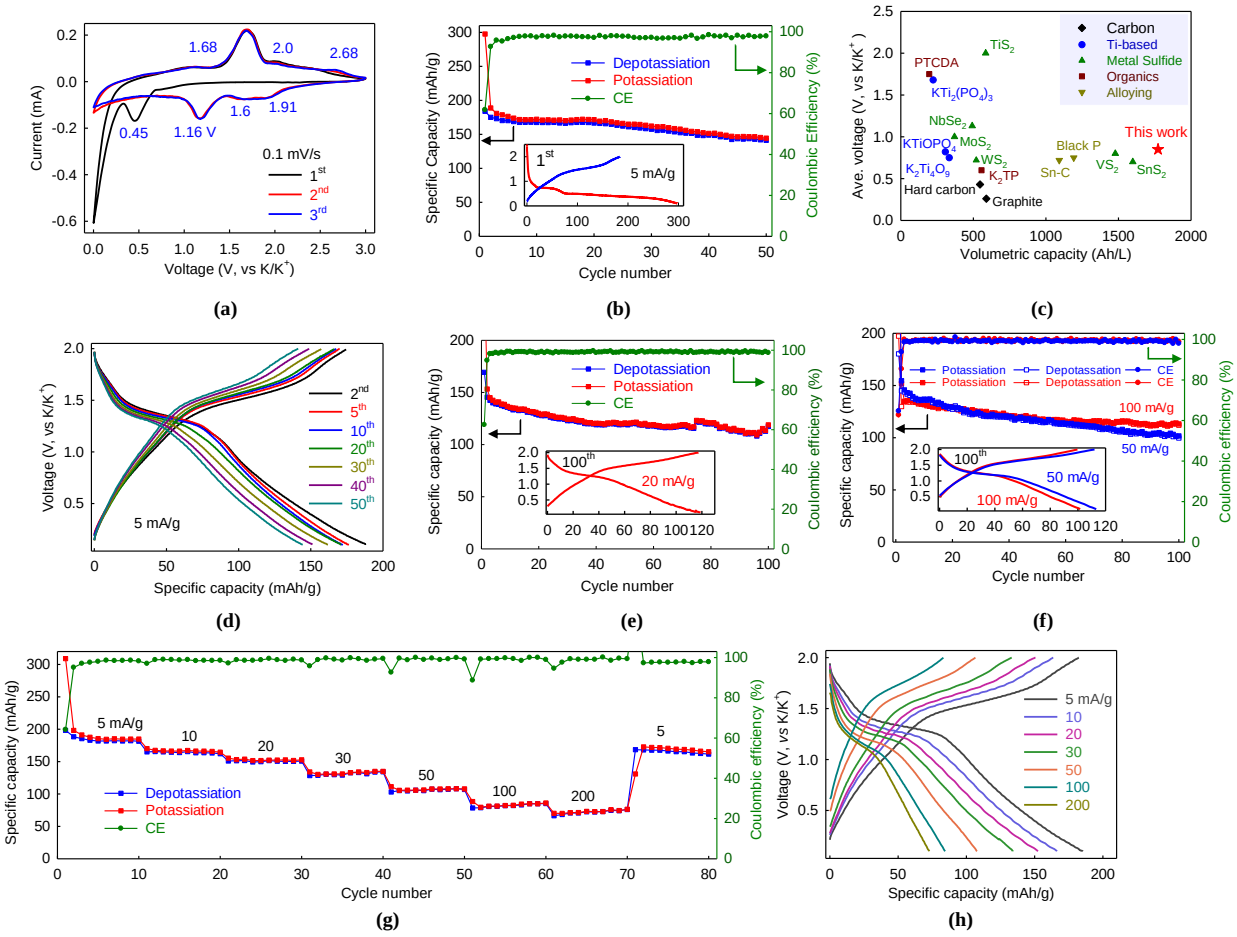

Fig. 2. (a) CV curves of the WSe_2 at 0.1 mV/s; (b) Cycling performance at 5 mA/g and the first-cycle voltage profile (inset); (c) Comparison of the volumetric capacity and average discharge voltage; (d) Voltage profiles of the 2nd, 5th, 10th, 20th, 30th, 40th, and 50th cycles at 5 mA/g; (e) Cycling performance of WSe_2 anode at 20 mA/g and the voltage profile at the 100th cycle (inset); (f) Cycling performance of the WSe_2 anode at 50 and 100 mA/g. Inset depicts the voltage profiles at the 100th cycle; (g, h) Rate capability and corresponding voltage profiles

We further conducted ex-situ XRD to investigate the underlying reaction mechanism. As shown in Fig. 3, the diffraction peaks at 13.6°, 31.4°, 37.8°, and 43.76° at the initial state (A point labeled in Fig. 3) correspond to (002), (100), (103), and (105) reflections of WSe_2, while the peaks at 38.47°, 44.78°, and 65.13° are the diffractions from the Al current collector (JCPDS no. 04-0850). Upon discharging to 0.5 V (B point), the diffraction peaks located at 13.6°, 31.4°, 37.8°, and 43.76° shift to 13.36°, 31.24°, 37.67°, and 41.5°, respectively. These peak shifts indicate the intercalation of K^+ ions into the interlayer of WSe_2 and an increase of interlayer spacing. Upon further discharging to 0.1 V (C point), the correlative characteristic peaks of WSe_2 disappear completely. Meanwhile, new peaks appear at 15.35°, 20.06°, 21.23°, 27.30°, and 28.46° and can be assigned to the (002), (211), (300), (322) and (132) lattice planes of K_2Se_4 (ICSD-430521). These observations indicate conversion-type reactions occurring during this step (from B to C). On reverse charging to 2 V (D point), the diffraction peaks associated with WSe_2 do not appear again, while new peaks at 23.52°, 24.23°, 31.01°, 34.02°, and 34.81° correspond well to the formation of Se (JCPDS no. 24-0714). According to these observations, the entire electrochemical reactions can be described as the following equations.

$$WSe_2 + xK^+ + xe^- \rightarrow K_xWSe_2 \text{ (discharging from 2 to 0.5 V)} \quad (1)$$

$$K_xWSe_2 + (2 - 2x)K^+ + (2 - 2x)e^- \rightarrow K_2Se_4 + 2W \text{ (discharging from 0.5 to 0.1 V)} \quad (2)$$

$$K_2Se_4 \rightarrow 4Se + 2K^+ + 2e^- \text{ (charging from 0.1 to 2 V)} \quad (3)$$

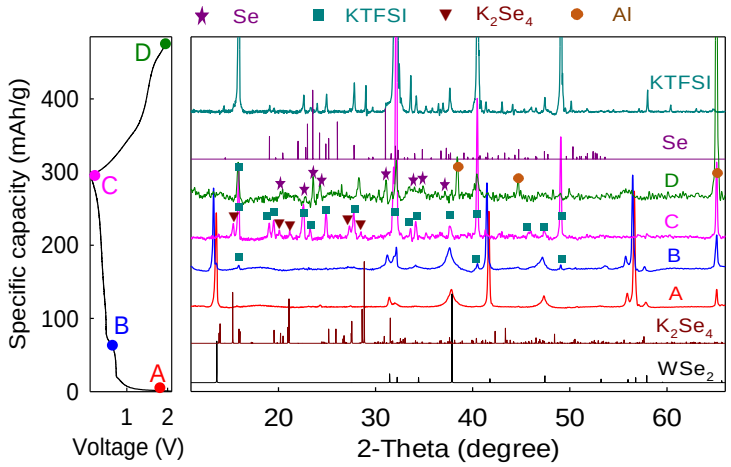

Fig. 3. Ex-situ XRD patterns of the WSe_2 electrode during the first cycle

It is noted that reactions (1) and (2) are irreversible, and after initial activation, the anode undergoes reversible conversion reactions between K_2Se_4 and Se, while the W metal formed during the initial cycle serves as an electron conductor to facilitate the conversion reactions.

We further fabricated proof-of-concept full-cell KIBs composed of an activated Prussian Blue cathode $K_{1.89}Mn[Fe(CN)_6]_{0.92}$[35] and an activated WSe_2 anode with a cathode-to-anode mass ratio of 1.8:1 (Fig. 4a). As depicted in Fig. 4b, the full-cell batteries operate at an average discharge voltage of 2.5 V and deliver a discharge capacity of 54.1 mAh/g and an energy density of 135.2 Wh/kg based on the total mass of the cathode and anode materials. After five cycles, the capacity and energy density remain at 45.8 mAh/g and 114.5 Wh/kg, respectively. This full-cell performance demonstrates the application prospect of the WSe_2 anode.

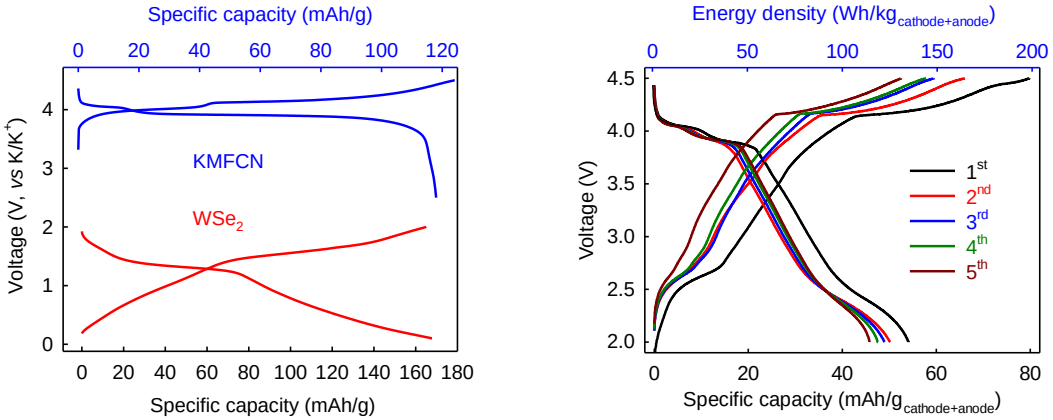

Fig. 4. (a) Voltage profiles of $K_{1.89}Mn[Fe(CN)_6]_{0.92}$ cathode and WSe_2 anode at 10 mA/g; (b) Electrochemical performance of the full-cell battery

4 CONCLUSION

In summary, we have revealed the intrinsic electrochemical behaviors of WSe_2. As an anode, WSe_2 exhibits an ultrahigh volumetric capacity of 1772.8 Ah/L at a current density of 5 mA/g, good rate capability (72 mAh/g at 200 mA/g), and long-term cyclability (83.14% capacity retention over 100 cycles at 100 mA/g). Through ex-situ XRD analysis we revealed that WSe_2 first undergoes intercalation reactions and subsequently conversion reactions to form K_2Se_4 and W during initial activation, and follows reversible conversion reactions between K_2Se_4 and Se in the subsequent cycles. Furthermore, full-cell KIBs utilizing the WSe_2 anode and a Prussian Blue cathode can provide an average discharge voltage of 2.5 V and an energy density of 135.2 $Wh/kg_{cathode+anode}$. WSe_2 may open new opportunities for the exploration of high-volumetric-capacity anode material in rechargeable potassium-ion batteries.

REFERENCES

(1) Li, M.; Lu, J.; Chen, Z.; Amine, K. 30 years of lithium-ion batteries. *Adv. Mater.* **2018**, 30, 1800561–24.

(2) Armand, M.; Tarascon, J. M. Building better batteries. *Nature* **2008**, 451, 652–657.

(3) Goriparti, S.; Miele, E.; De Angelis, F.; Di Fabrizio, E.; Zaccaria, R. P.; Capiglia, C. Review on recent progress of nanostructured anode materials for Li-ion batteries. *J. Power Sources* **2014**, 257, 421–443.

(4) Komaba, S.; Hasegawa, T.; Dahbi, M.; Kubota, K. Potassium intercalation into graphite to realize high-voltage/high-power potassium-ion batteries and potassium-ion capacitors. *Electrochem. Commun.* **2015**, 60, 172–175.

(5) Wang, G.; Xiong, X. H.; Xie, D.; Lin, Z. H.; Zheng, J.; Zheng, F. H.; Li, Y. P.; Liu, Y. Z.; Yang, C. H.; Liu, M. L. Chemically activated hollow carbon nanospheres as a high-performance anode material for potassium ion batteries. *J. Mater. Chem. A* **2018**, 6, 24317–24323.

(6) Chu, S.; Cui, Y.; Liu, N. The path towards sustainable energy. *Nat. Mater.* **2016**, 16, 16–22.

(7) He, H.; Man, Y.; Yang, J.; Xie, J.; Xu, M. MoO_2 nanosheets embedded in amorphous carbon matrix for sodium-ion batteries. *Roy. Soc. Open Sci.* **2017**, 4, 170892–7.

(8) Ren, X.; Zhao, Q.; McCulloch, W. D.; Wu, Y. MoS_2 as a long-life host material for potassium ion intercalation. *Nano Research* **2017**, 10, 1313–1321.

(9) Zhang, R.; Bao, J.; Pan, Y.; Sun, C. F. Highly reversible potassium-ion intercalation in tungsten disulfide. *Chem. Sci.* **2019**, 10, 2604–2612.

(10) Yu, X. Y.; Hu, H.; Wang, Y.; Chen, H.; Lou, X. W. Ultrathin MoS_2 nanosheets supported on N-doped carbon nanoboxes with enhanced lithium storage and electrocatalytic properties. *Angew. Chem. Int. Ed.* **2015**, 54, 7395–7398.

(11) Wu, R.; Wang, D. P.; Rui, X.; Liu, B.; Zhou, K.; Law, A. W.; Yan, Q.; Wei, J.; Chen, Z. *In-situ* formation of hollow hybrids composed of cobalt sulfides embedded within porous carbon polyhedra/carbon nanotubes for high-performance lithium-ion batteries. *Adv. Mater.* **2015**, 27, 3038–3044.

(12) Jiao, X.; Liu, X.; Wang, B.; Wang, G.; Wang, X.; Wang, H. A controllable strategy for the self-assembly of WM nanocrystals/nitrogen-doped porous carbon superstructures (M = O, C, P, S, and Se) for sodium and potassium storage. *J. Mater. Chem. A* **2020**, 8, 2047–2065.

(13) Zhang, R.; Huang, J.; Deng, W.; Bao, J.; Pan, Y.; Huang, S.; Sun, C. F. Safe, low-cost, fast-kinetics and low-strain inorganic-open-framework anode for potassium-ion batteries. *Angew. Chem. Int. Ed.* **2019**, 58, 16474–16479.

(14) Mao, M.; Cui, C.; Wu, M.; Zhang, M.; Gao, T.; Fan, X.; Chen, J.; Wang, T.; Ma, J.; Wang, C. Flexible ReS_2 nanosheets/N-doped carbon nanofibers-based paper as a universal anode for alkali (Li, Na, K) ion battery. *Nano Energy* **2018**, 45, 346–352.

(15) Xu, B.; Ma, X.; Tian, J.; Zhao, F.; Liu, Y.; Wang, B.; Yang, H.; Xia, Y. Layer-structured $NbSe_2$ anode material for sodium-ion and potassium-ion batteries. *Ionics* **2019**, 25, 4171–4177.

(16) Wu, M.; Yang, J.; Ng, D. H. L.; Ma, J. Rhenium diselenide anchored on reduced graphene oxide as anode with cyclic stability for potassium-ion battery. *Phys. Status Solidi Rapid Res. Lett.* **2019**, 13, 1900329–7.

(17) Wang, W.; Jiang, B.; Qian, C.; Lv, F.; Feng, J.; Zhou, J.; Wang, K.; Yang, C.; Yang, Y.; Guo, S. Pistachio-shuck-like $MoSe_2$/C core/shell nanostructures for high-performance potassium-ion storage. *Adv. Mater.* **2018**, 30, 1801812–7.

(18) Sun, C. F.; Hu, J.; Wang, P.; Cheng, X. Y.; Lee, S. B.; Wang, Y. Li_3PO_4 matrix enables a long cycle life and high energy efficiency bismuth-based battery. *Nano Lett.* **2016**, 16, 5875–5882.

(19) Sun, C. F.; Zhu, H.; Okada, M.; Gaskell, K.; Inoue, Y.; Hu, L.; Wang, Y. Interfacial oxygen stabilizes composite silicon anodes. *Nano Lett.* **2015**, 15, 703–708.

(20) Jian, Z.; Luo, W.; Ji, X. Carbon electrodes for K-ion batteries. *J. Am. Chem. Soc.* **2015**, 137, 11566–11569.

(21) Fan, H. N.; Wang, X. Y.; Yu, H. B.; Gu, Q. F.; Chen, S. L.; Liu, Z.; Chen, X. H.; Luo, W. B.; Liu, H. K. Enhanced potassium ion battery by inducing interlayer anionic ligands in $MoS_{1.5}Se_{0.5}$ nanosheets with exploration of the mechanism. *Adv. Energy Mater.* **2020**, 10, 1904162–9.

(22) Jian, Z.; Xing, Z.; Bommier, C.; Li, Z.; Ji, X. Hard carbon microspheres: potassium-ion anode versus sodium-ion anode. *Adv. Energy Mater.* **2016**, 6, 1501874–5.

(23) Hu, X.; Liu, Y.; Chen, J.; Yi, L.; Zhan, H.; Wen, Z. Fast redox kinetics in Bi-heteroatom doped 3*D* porous carbon nanosheets for high-performance hybrid potassium-ion battery capacitors. *Adv. Energy Mater.* **2019**, 9, 1901533–10.

(24) Alvin, S.; Cahyadi, H. S.; Hwang, J.; Chang, W.; Kwak, S. K.; Kim, J. Revealing the intercalation mechanisms of lithium, sodium, and potassium in hard carbon. *Adv. Energy Mater.* **2020**, 10, 2000283–16.

(25) Fan, L.; Ma, R.; Wang, J.; Yang, H.; Lu, B. An ultrafast and highly stable potassium-organic battery. *Adv. Mater.* **2018**, 30, 1805486–8.

(26) Fan, L.; Ma, R.; Zhang, Q.; Jia, X.; Lu, B. Graphite anode for a potassium-ion battery with unprecedented performance. *Angew. Chem. Int. Ed.* **2019**, 58, 10500–10505.

(27) Han, J.; Niu, Y.; Bao, S. J.; Yu, Y. N.; Lu, S. Y.; Xu, M. Nanocubic $KTi_2(PO_4)_3$ electrodes for potassium-ion batteries. *Chem. Commun.* **2016**, 52, 11661–11664.

(28) Kishore, B.; Venkatesh, G.; Munichandraiah, N. $K_2Ti_4O_9$: a promising anode material for potassium ion batteries. *J. Electrochem. Soc.* **2016**, 163, A2551–A2554.

(29) Lakshmi, V.; Chen, Y.; Mikhaylov, A. A.; Medvedev, A. G.; Sultana, I.; Rahman, M. M.; Lev, O.; Prikhodchenko, P. V.; Glushenkov, A. M. Nanocrystalline SnS_2 coated onto reduced graphene oxide: demonstrating the feasibility of a non-graphitic anode with sulfide chemistry for potassium-ion batteries. *Chem. Commun.* **2017**, 53, 8272–8275.

(30) Lei, K.; Li, F.; Mu, C.; Wang, J.; Zhao, Q.; Chen, C.; Chen, J. High K-storage performance based on the synergy of dipotassium terephthalate and ether-based electrolytes. *Energy Environ. Sci.* **2017**, 10, 552–557.

(31) Sultana, I.; Rahman, M. M.; Ramireddy, T.; Chen, Y.; Glushenkov, A. M. High capacity potassium-ion battery anodes based on black phosphorus. *J. Mater. Chem. A* **2017**, 5, 23506–23512.

(32) Sultana, I.; Ramireddy, T.; Rahman, M. M.; Chen, Y.; Glushenkov, A. M. Tin-based composite anodes for potassium-ion batteries. *Chem. Commun.* **2016**, 52, 9279–9282.

(33) Wang, L.; Zou, J.; Chen, S.; Zhou, G.; Bai, J.; Gao, P.; Wang, Y.; Yu, X.; Li, J.; Hu, Y. S.; Li, H. TiS_2 as a high performance potassium ion battery cathode in ether-based electrolyte. *Energy Storage Mater.* **2018**, 12, 216–222.

(34) Zhou, J.; Wang, L.; Yang, M.; Wu, J.; Chen, F.; Huang, W.; Han, N.; Ye, H.; Zhao, F.; Li, Y.; Li, Y. Hierarchical VS_2 nanosheet assemblies: a universal host material for the reversible storage of alkali metal ions. *Adv. Mater.* **2017**, 29, 1702061–8.

(35) Xue, L.; Li, Y.; Gao, H.; Zhou, W.; Lu, X.; Kaveevivitchai, W.; Manthiram, A.; Goodenough, J. B. Low-cost high-energy potassium cathode. *J. Am. Chem. Soc.* **2017**, 139, 2164–2167.